# A Calculation Evidence on Staged Mott and Peierls Transitions in VO 2 Revealed by Mapping Reduced-Dimension Potential Energy Surface

**ARTICLE** *in* JOURNAL OF PHYSICAL CHEMISTRY LETTERS · SEPTEMBER 2015

Impact Factor: 7.46 · DOI: 10.1021/acs.jpclett.5b01376



**4 AUTHORS**, INCLUDING:

Shi Chen

Friedrich-Alexander-University of Erlangen-…

**11** PUBLICATIONS **124** CITATIONS

SEE PROFILE

Jianjun Liu

Chinese Academy of Sciences

**22** PUBLICATIONS **71** CITATIONS

SEE PROFILE

THE JOURNAL OF PHYSICAL CHEMISTRY Letters

Letter

pubs.acs.org/JPCL

# Calculation Evidence of Staged Mott and Peierls Transitions in $VO_2$ Revealed by Mapping Reduced-Dimension Potential Energy Surface

Shi Chen,[†,‡] Jianjun Liu,[*,†] Hongjie Luo,[†,‡] and Yanfeng Gao[*,†,‡]

[†]State Key Laboratory of High Performance Ceramics and Superfine Microstructure, Shanghai Institute of Ceramics, Chinese Academy of Sciences, 1295 Dingxi Road, Shanghai 200050, China

[‡]School of Materials Science and Engineering, Shanghai University, 99 Shangda Road, Shanghai 200444, China

Supporting Information

**ABSTRACT:** Unraveling the metal−insulator transition (MIT) mechanism of $VO_2$ becomes tremendously important for understanding strongly correlated character and developing switching applications of $VO_2$. First-principles calculations were employed in this work to map the reduced-dimension potential energy surface of the MIT of $VO_2$. In the beginning stage of MIT, a significant orbital switching between $\sigma$-type $d_{z^2}$ and $\pi$-type $d_{x^2-y^2}/d_{yz}$ accompanied by a large V−V dimerization and a slight twisting angle change opens a band gap of ~0.2 eV, which can be attributed to the electron-correlation-driven Mott transition. After that, the twisting angle of one chain quickly increases, which is accompanied by the appearance of a larger change in band gap from 0.2 to 0.8 eV, even though orbital occupancy is maintained. This finding can be ascribed to the structure-driven Peierls transition. The present study reveals that a staged electron-correlation-driven Mott transition and structure-driven Peierls transition are involved in MIT of $VO_2$.

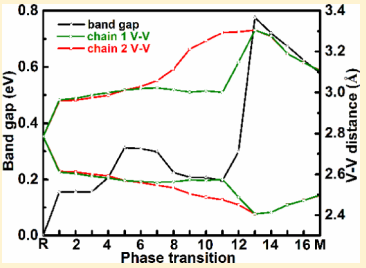




Vanadium dioxide ($VO_2$), a strongly correlated electron and metal−insulator transition (MIT) material, has been attracting a significant interest in fundamental scientific research and developing advanced technological applications.[1−10] The transition is characterized by a crystal structure change from high-temperature tetragonal $P4_2/mnm$ to low-temperature monoclinic $P2_1/c$ at 340 K corresponding to V−V dimerization along the $c$ axis forming homopolar bonds and undergoing a structural twist measured by Jahn−Teller distortion angle change of edge-sharing octahedral $VO_6$.[11] An electron-correlation-driven Mott transition,[12,13] and a structure-distortion-driven Peierls transition,[14−16] or cooperation of two mechanisms,[8,17] have been proposed. Because a delicate interplay between crystal structure and electronic correlation occurs during the MIT process, the driving force behind MIT still remains unclear and has been a topic of controversy. In addition, the MIT can be distinguished by abrupt and dramatic changes in the electrical and optical properties, offering many opportunities for scientific development as well as potential applications of $VO_2$ in smart optical and electrical switchers.[18−20] Practical utilities of the previously mentioned applications critically depend on the fundamental understanding of the MIT.[7,8]

The different underlying physical mechanisms such as an electron-correlation-driven Mott transition,[12,13] a structure-driven Peierls transition,[14−16] and the cooperation of these two mechanisms[8,17] have been proposed based on spatial-, spectral-, temperature-, and time-resolved techniques. Yao et al. combined in situ X-ray absorption fine structure (XAFS) technique and first-principles calculations to study the detailed evolution of the V−V dimerization, the twisting angle $\delta$, and the electric conductivity change during MIT, in which electron-correlation studies are not enough to elucidate the Mott transition mechanism of MIT.[8] The combination of near-field infrared microscopy and far-field infrared spectroscopy revealed the Mott transition with divergent quasi-particle mass in the metallic puddles at the onset of MIT.[12] Haverkort et al. presented a direct experimental evidence for orbital switching of V 3d states across MIT, establishing Peierls-like transition mechanism.[15] By using X-ray absorption spectroscopy with high spectral, spatial, and temperature resolution, Kumar et al. recently found that a predominantly Mott-like transition precedes a Peierls transition across the heating and cooling processes and there exist different intermediate states;[7] however, such a temperature-dependent spectroscopy study is lack of the intrinsic structural exploration (V chains, V−V and $\delta$), which naturally hinders the deep comprehension of the MIT. In fact, many experiments on the MIT of $VO_2$ employed measurement samples that are different in the morphology, particle size, or stress, leading to distinct findings.[7,8] Certainly it is very challenging to record the change of the V−V and $\delta$ as well as electron correlation from temperature-resolution experiments.

Despite significant improvement in understanding of the MIT of $VO_2$, some puzzles still require being unraveled. In general, the first-principles theoretical studies are able to provide a synchronized characterization for structural evolution and electron correlation change in $VO_2$ MIT; however, most of

**Received:** June 28, 2015
**Accepted:** September 2, 2015

  

DOI: 10.1021/acs.jpclett.5b01376
J. Phys. Chem. Lett. 2015, 6, 3650−3656

Table 1. Calculated and Experimental Lattice Parameters for $VO_2$ (R/M1)

| $VO_2$ | $a$ (Å) | $b$ (Å) | $c$ (Å) | $\alpha$ (deg) | $\beta$ (deg) | $\gamma$ (deg) | type |
|---|---|---|---|---|---|---|---|
| R | 4.609 | 4.609 | 2.785 | 90.0 | 90.0 | 90.0 | cal. |
| R | 4.554 | 4.554 | 2.857 | 90.0 | 90.0 | 90.0 | exp.[37] |
| tetragonal $R_{red}$ | 5.571 | 4.609 | 4.609 | 90.0 | 90.0 | 90.0 | cal. |
| monoclinic $R_{red}$ | 5.571 | 4.609 | 5.385 | 90.0 | 121.2 | 90.0 | cal. |
| M1 | 5.610 | 4.571 | 5.393 | 90.0 | 121.9 | 90.0 | cal. |
| M1 | 5.753 | 4.526 | 5.383 | 90.0 | 122.6 | 90.0 | exp.[37] |

theoretical studies were focused on evaluation of various density functional theory methods implemented in strongly correlation systems.[21−23] Some computation studies were performed to reveal electron−phonon interactions, in which the electron−electron and electron−lattice interactions are neglected.[24] Previous studies showed that the V−V bond distance and twisting angle $\delta$ are involved in the structural evolution of MIT.[8] It is necessary to map a reduced-dimension potential energy surface describing structural evolution and generating electron structure information by following a lowest-energy transition path.

In this work, we simulated the phase transition from $VO_2$ (R) to $VO_2$ (M1) and performed an extensive search for the minimum energy path of $VO_2$ phase transition. Furthermore, we calculated along the minimum energy path and obtained the relaxed structure, total energy, and band gap of these transition states. A total comparison between these calculated variables was carried out to reveal the change of V chains and their effects on energy and band gap.

As a strongly correlated material, the distribution of localized d-electrons occupation in $VO_2$ may form different bonding mechanisms such as dispersive metallic bonding of R and singlet bonding of M1 as well as various magnetic phases. The subtle interplay between electronic, magnetic, and structural properties leads to the relative stability of various $VO_2$ phases, which sensitively depends on the energy functionals used in theoretical calculations.[21] On the basis of density functional theory (DFT), the different energy functionals such as LDA,[21] GGA,[25] LDA+U,[26] PBE+U,[8,27] HSE,[22,23] LDA+DMFT,[28,29] and GW[30,31] have been applied to understand MIT mechanisms. Recently, Yuan et al. of our group performed systematic studies on relative stability of various structural and magnetic phases by using LDA, LDA+U, PBE, PBE+U, and HSE methods. On the basis of their calculations, PBE+U with nonmagnetic solution can give the most reasonable energy stability (table 1 in ref 21) and generate the reasonable electronic structure properties of $VO_2$ (R), $VO_2$ (M1), and $VO_2$ (M2) phases.[21] The energy difference between R and M1 phases was calculated to be 35.7 meV per $VO_2$ formula unit, which is very close to the experimental heat (44 meV).[32] Our present work and previous studies[21] indicate that PBE+U (LDA+U) can give metallic state formed by dispersive bands of lone d electrons of V. The calculated band order is consistent with GW calculations.[31] The on-site Coulomb repulsive parameter (U) is effective to open the insulating gap of $VO_2$ (M1), although PBE+U predicted the antiferromagnetic state of ground-state $VO_2$ (M1) phase, which is different from $VO_2$ (M1) of no local magnetic moment observed in experiments.[21] Fortunately, the basic band structure characters is maintained by comparing with more sophisticated methods (GW[30] and DFT-DMFT[28]). In the present work, we focus on the description of energy evolution and electronic structure during MIT. Therefore, PBE+U functional with spin-unpolarization solution (nonmagnetic state) was used in our potential energy scan and electronic structure calculations.

In addition, the spin-unpolarization calculations were chosen to simulate $VO_2$ (R) and $VO_2$ (M1) structures, which is mainly attributed to nonmagnetic state of $VO_2$ (M1) and the calculated relative stability between $VO_2$ (R) and $VO_2$ (M1). The $VO_2$ (R) phase is experimentally observed as paramagnetic state with a weak local magnetic moment,[33] which is consistent with PBE+U calculations;[21] however, a consistent computational functional (PBE+U with a nonmagnetic solution) is greatly important to yield a smooth potential energy surface during MIT and observe a rational and continual electronic structure evolution. In particular, our band structure analysis was performed by referring spin-polarization density of states (DOS) calculations for some points near R phases to ensure a reasonable description for electronic structure evolution.

Periodic DFT calculations using the PBE functional were performed using the VASP code.[34,35] To improve the treatment of electronic correlations in our DFT calculations, we took into account the Hubbard on-site repulsion U within the so-called GGA+U approximation.[36] The effective strength ($U_{eff}$, $U_{eff} = U - J$) of the on-site Coulomb correlation was set at 3.2 eV, in which $U$ (3.9 eV) is the on-site Hubbard repulsion and $J$ (0.7 eV) is Hund's exchange interaction. The similar $U$ and $J$ values have been used in the other publication, showing a reliable calculation results.[25] The electron−ion interactions were described by projector-augmented wave (PAW) potential. An energy cutoff of 400 eV and 4 × 4 × 4 k-point Monkhorst−Pack grid were used. The convergence criterion of energy and structural relaxation were set as less than $1.0 \times 10^{-6}$ eV and 0.01 eV/Å, respectively. In the phase-transition calculation process from $VO_2$ (R) to $VO_2$ (M1), the structural relaxation of each intermediate phase was calculated on the basis of the atomic position of previous intermediate phase.

To check for the reliability of computational methods, especially for the selected energy functional (PBE+U) with the on-site Coulomb correlation effect, we calculated the lattice parameters, atomic coordinates, and band gaps of R and M1 species for comparison with experiments. The calculated and experimental lattice parameters for $VO_2$ (R/M1) are summarized in Table 1. The lattice parameters of $VO_2$ (R/M1) from first-principles calculation match well with the experimental data.[37] Our calculations indicate that the tetragonal rutile-type $VO_2$ (R) along the $c$ axis with equidistant vanadium atoms ($R_{V-V}$ = 2.785 Å) gives rise to a monoclinic phase $VO_2$ (M1) along the $a$ axis with alternative V−V bond distances of 2.509 and 3.133 Å in Figure 1a,c. The bond distances are consistent with the previous experimental study.[8] In terms of electronic structure, our PBE+U calculation for M1 phase obtains the band gap of 0.58 eV, which is in good agreement with experimental results.[38] All tests show that our computational methods are reliable to reveal structural and electronic properties of $VO_2$ phase transition.





DOI: 10.1021/acs.jpclett.5b01376
J. Phys. Chem. Lett. 2015, 6, 3650−3656

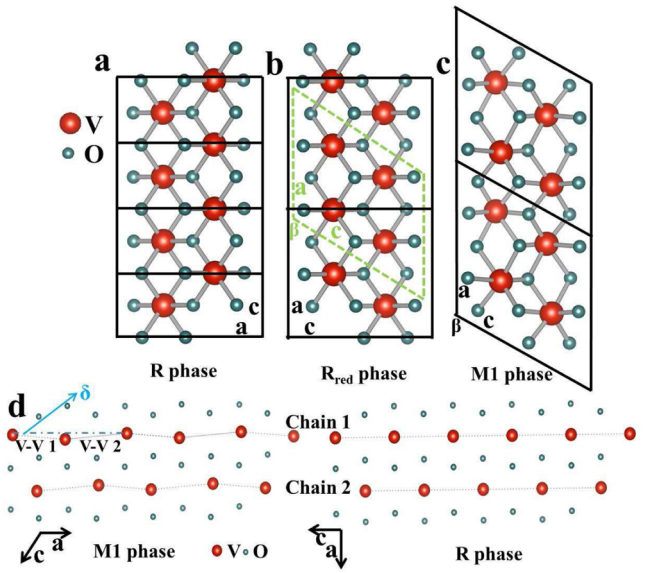


**Figure 1.** Calculated structure of $VO_2$ (R/M1). (a) $VO_2$ (R) unit cell. (b) $VO_2$ ($R_{red}$) unit cell, redefinition of the lattice parameters of $VO_2$ (R) from tetragonal (black solid line) and monoclinic (dotted green line) view, respectively. (c) $VO_2$ (M1) unit cell. (d) Definition of V−V1distance, V−V2 distance, and $\delta$ angle in the V chains in the $VO_2$ phase-transition process.

The MIT can be characterized by the crystal structure transformation from a high-temperature tetragonal rutile (R) structure containing a single V−V bond distance and linear chains of edge-shared Jahn−Teller-distorted $VO_6$ octahedra, to a low-temperature monoclinic (M1) structure containing $V^{4+}$−$V^{4+}$ pairs forming zigzag chains with alternating V−V distances and more distorted $VO_6$ octahedra. Although there is a large change in bond distance from 2.785 Å in R to 2.509 and 3.133 Å in M1, the changes of crystal lattices are delicate. To better compare the lattice parameters of $VO_2$ (R/M1), we redefined the lattice parameters for $VO_2$ (R) from tetragonal and monoclinic view, respectively, in Figure 1b, and the obtained parameters are listed in Table 1. Obviously, there was a slight difference between $VO_2$ (M1) and monoclinic redefined $VO_2$ (R) ($VO_2$ ($R_{red}$)) in the lattice parameters. The $\beta$ difference just reached 0.7° and the lattice differences ($\Delta a$ = 0.039 Å, $\Delta b$ = −0.038 Å, and $\Delta c$ = 0.008 Å) were smaller than 0.039 Å. The delicate lattice change under monoclinic symmetry cannot be accurately described by the DFT-based first-principles calculations.

Besides thermal effect,[18] different external stimuli such as stress,[39] doping,[40] optical field,[24] and magnetic field[41] can trigger the MIT of $VO_2$. Some external interactions may cause a large lattice change, which indicates the possible existence of various transition paths from R to M1 phases.[40] As shown in Figure 1d, the V−V dimerization and the distortion of $VO_6$ octahedra in these transformations take place along $a$ axis and in the $a$−$c$ plane, respectively. Previous studies showed that the V−V bond distance and $\delta$ twisting angle in the V chains are key characteristics for $VO_2$ phase transition to determine the structural and electronic properties of different $VO_2$ phases.[8,40] The paired V−V formation directly leads to splitting half-filled $d_{||}$ orbital in R phase into fully filled orbital ($d_{||}$) and empty orbital ($\pi^*$), indicating the occurrence of a metal to semiconductor transition.[42] Moreover, there existed two apparent distinctions ($\Delta c$ = 0.784 Å, $\Delta\beta$ = 31.9°) and two small differences ($\Delta a$ = 0.039 Å, $\Delta b$ = −0.038 Å) between $VO_2$ (M1) and tetragonal redefined $VO_2$ (R). As a result, the lattice parameters of $c$ and $\beta$ are dominant variation during the MIT of $VO_2$, and the change of other parameters is small and neglected.

For a martensitic solid−solid phase transformation, the activated processes include the deformation of cell vectors and collective atomic motion, both of which may couple each other in a local space, but we assume that atomic motion is much faster than bulk crystal reshaping, which is similar to a spirit of Born−Oppenheimer approximation. Because atomic coordinates in $VO_2$ do not experience a large change, we performed a coupling calculation in which the cell vectors are scanned and atomic coordinates are allowed to relax during cell vector change. In this method, the calculated trajectory provides the minimum energy path (MEP) of phase transition. As a result, a 2D potential energy surface as a function of $c$ and $\beta$ is mapped in Figure 2. The minimum energy transition path along which

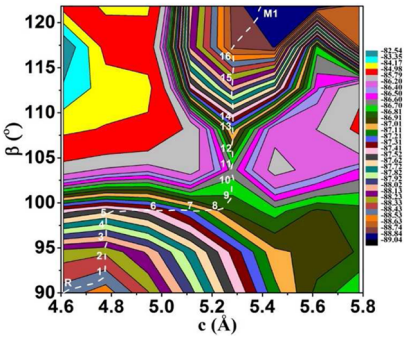


**Figure 2.** Calculated 2D potential energy surface of $VO_2$ intermediate phases as a function of $c$ and $\beta$. The color bar on the right denotes the energy level (eV/unit). The white dotted line and the white numbers stand for the minimum energy path and the intermediate phases in the $VO_2$ phase transition.

structural and electronic evolution can be explored is depicted (white dashed line) in our calculated surfaces. The computation started from $VO_2$ (R) and gradually reached $VO_2$ (M1). After the step-by-step atomic relaxation, the finally derived $VO_2$ (M1) was extremely similar to the directly calculated $VO_2$ (M1) in terms of the V chains, band gap, and energy in Table S1, confirming calculation rationality. Along the minimum energy path, the total energy increased from −88.481 eV (R) to −86.581 eV (11) and then decreased to −88.961 eV (M1), indicating that a high-energy transition state occurs in $c$ = 5.28 Å and $\beta$ = 104.1°.

To elucidate MIT mechanism, the detailed structural dynamics, band gap evolution, and total energy change along this minimum energy path were plotted in Figure 3. As shown in Figure 3a,b, two chains in the start and end of the minimum energy path underwent a consistent structural variation in terms of V−V bond distance and twisting angle $\delta$; however, in the stage of (6)−(13), two chains presented nonuniform structural evolution, forming two different polar chains. This phenomenon could be also observed experimentally in the intermediate phase of $VO_2$ (M2), in which only half of the V atoms dimerize, while the other half form chains of equally spaced atoms behaving as spin-1/2 Heisenberg chains. For comparison, the calculated structure of M2 phase is displayed in Figure S1. The insulating M2 exists as a metastable phase and could be stabilized to M1 phase by stress.[43,44] In addition, the




DOI: 10.1021/acs.jpclett.5b01376
J. Phys. Chem. Lett. 2015, 6, 3650−3656

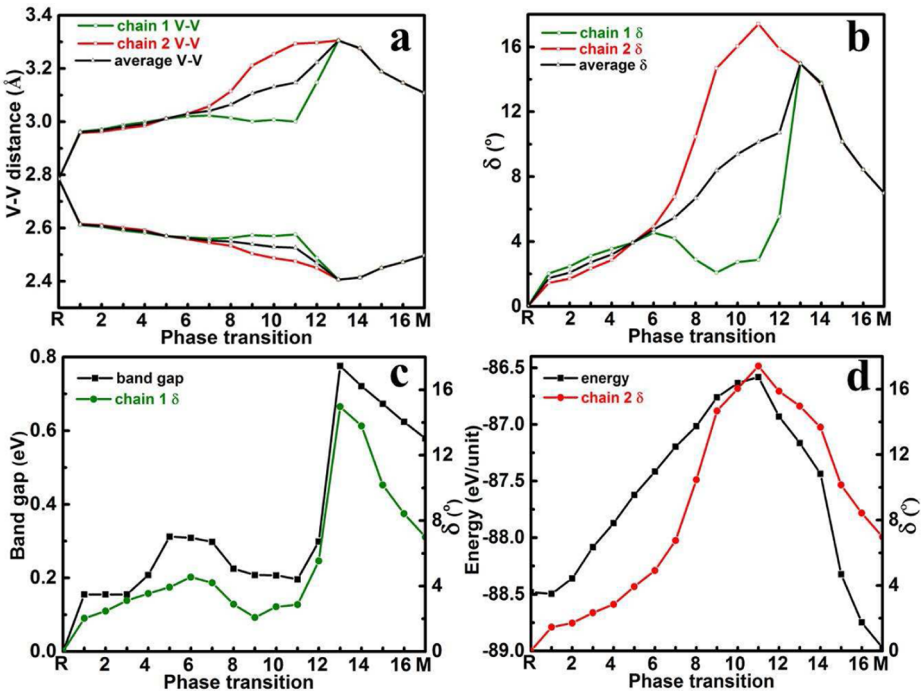


**Figure 3.** Calculated structure, energy, and bandgap. (a) The V−V distances and their average values of the V chains in the $VO_2$ phase transition. (b) The $\delta$ and their average values of the V chains in the $VO_2$ phase transition. (c) The band gap and $\delta$ in the V chain 1 in the $VO_2$ phase transition. (d) The energy and $\delta$ in the V chain 2 in the $VO_2$ phase transition.

equidistant V−V bond in the metal R phase has a very fast change (which only occurs in the first step) into alternatively short and long bond distances, forming a bipolar chain. In contrast, the twisting angle $\delta$ seems to experience a gradual change.

It is of importance to correlate the band gap evolution of $VO_2$ with the local structure change described by the V−V bond distance and twisting angle $\delta$ and with electron-correlation interactions described by orbital switching. These correlations can unravel the contribution of Peierls and Mott transition on MIT dominated by electron−phonon and electron−electron interactions, respectively. First of all, the evolution of twisting angle $\delta$ in chain 1 ($\delta$1) exhibits an excellent consistence with the band gap change of $VO_2$ from R to M1 in Figure 3c. To be specific, two local peaks existed in band gap, which was also observed at the close location for the $\delta$1. Second, the $\delta$ in chain 2 ($\delta$2) and total energy exhibit a similar change tendency, as shown in Figure 3d. Third, the highest-energy point (11) is presented when the V−V bond distance and twisting angle $\delta$ in chain 2 reach maximum values but not in chain 1.

There are two obvious band gap increases (0 → 0.2 eV and 0.2 → 0.8 eV) at the 0−1 and 11−13 steps, respectively. During 1−11 steps, the band gaps of $VO_2$ have the oscillation around 0.2 eV. In this stage, the V−V bond distances and twisting angle $\delta$ in chain 1 did not change largely, whereas those in chain 2 gradually increased. Previous studies indicated that the V−V dimerization and twisting angle $\delta$ are regarded as the characteristic parameters of electron-correlation-driven Mott transition and structure-driven Peierls transition.[8] To elucidate the possible driving forces behind MIT corresponding to two band gap increases, we further calculated the total and projected densities of states (DOS) of six characteristic points (R → 1→2 → 11 → 13 → M1) along the minimum-energy transition path, which were plotted in Figure 4. In our calculated R phase, electrons around Fermi level occupy $e_g$-state $d_{z^2}$ orbital ($\sigma$) and $t_{2g}$-state $d_{x^2-y^2}$ orbital ($\pi$). The former has a higher occupant number than the latter. The significant dimerization (from 2.79 to 2.96 Å and 2.61 Å) in V−V and a slight twisting of $\delta$ (2°) corresponding to 1 step open the band gap of around 0.2 eV. Very importantly, there are significant orbital switching phenomena occurred from R to 1. At step 1, electrons dominantly occupy the $d_{x^2-y^2}$ orbital ($\pi$) and second $d_{yz}$ orbital ($\pi$). In contrast, fewer electrons occupy the $d_{z^2}$ orbital ($\sigma$). More importantly, such an electronic structure characteristic remains from step 1 to step final M1 even though there are more significant changes in structure and band gap (0.2 to 0.8 eV). Therefore, it is concluded that the band gap change of 0 to 0.2 eV should be attributed to electron-correction-driven Mott transition in which orbital switching between $\sigma$ and $\pi$ states makes a significant contribution. In fact, such an orbital-assisted MIT in $VO_2$ was observed experimentally by soft-X-ray absorption spectroscopy.[15] Furthermore, the band gap change of 0.2 to 0.8 eV that occurred at the steps of 11−13 should be ascribed to structure-driven Peierls transition due to a large $\delta$ change and V−V dimerization. In this stage, orbital occupancy does not change in nature. Therefore, a staged electronic and structural transition mechanism regulates the R → M1MIT of $VO_2$. Further more, it indicates that mapping potential energy surface and electronic/structural analysis is an effective strategy to reveal the underlying mechanism of MIT of $VO_2$.

In fact, cohesive electron and structure transition mechanism has been proposed by several research groups.[8,12−15,17] However, ultrafast transition processes in their own phase space and significant mixing character make it difficult to distinguish each other. Very recently, Kumar proposed sequential electronic and structural transitions in $VO_2$ based on X-ray absorption spectromicroscopy.[7] Although our calculations based on the lattice change may be related to





DOI: 10.1021/acs.jpclett.5b01376
J. Phys. Chem. Lett. 2015, 6, 3650−3656

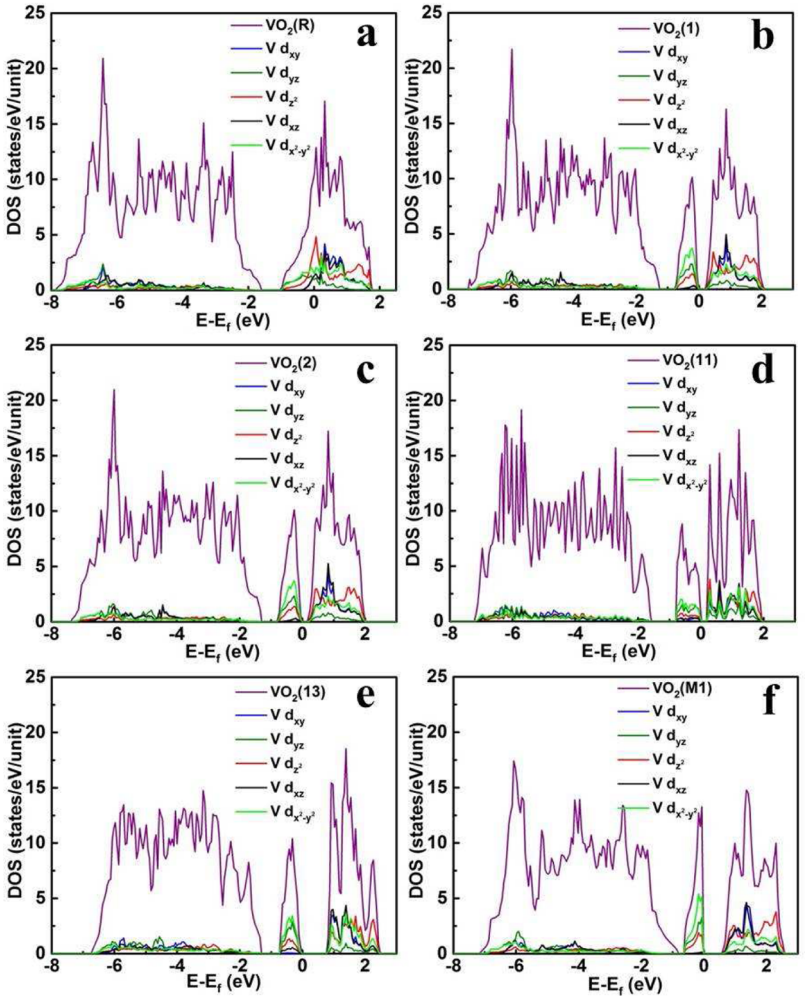


**Figure 4.** Total and projected density of state (DOS) of six characteristic points (R (a) → 1 (b) → 2 (c) → 11 (d) →13 (e) →M1 (f)) along minimum-energy transition path.

stress-like external force, the revealed sequential transition mechanism, electronic transition followed by structural transition, is consistent with experimental observation of $VO_2$ phase transition by temperature.

In this work, DFT-based first-principles calculations were carried out to map a reduced-dimension potential energy surface of the MIT of $VO_2$, which was used to analyze the underlying MIT mechanism by correlating band gap change with orbital occupancy and structure change. A transition-state structure that is similar to M2 phase and has two different polar chains is discovered along the minimum-energy transition path. Two neighboring chains show different structural evolution modes that can be correlated to band gap and energy changes, respectively. During phase transition, there are two band gaps that open stages corresponding to 0 to 0.2 and 0.2 to 0.8 eV. In the beginning stage of MIT, a significant orbital switching between $\sigma$-type $d_{z^2}$ and $\pi$-type $d_{x^2-y^2}/d_{yz}$ accompanied by a large V−V dimerization and a slight twisting angle change opens a band gap of ∼0.2 eV. After the transition state, the twisting angle of one chain quickly increases, which directly corresponds to a larger change in band gap from 0.2 to 0.8 eV, even though orbital occupancy is maintained. Our calculations indicate that the staged electron-correlation-driven Mott transition and structure-driven Peierls transition occur in the MIT of $VO_2$.

## ■ ASSOCIATED CONTENT

### Supporting Information

The material is available free of charge via the Internet The Supporting Information is available free of charge on the ACS Publications website at DOI: 10.1021/acs.jpclett.5b01376.

The comparison of the finally derived $VO_2$ (M1) and the directly calculated $VO_2$ (M1) and the projected structure of $VO_2$ (M2). (PDF)

## ■ AUTHOR INFORMATION

### Corresponding Authors

*J.L.: E-mail: jliu@mail.sic.ac.cn.
*Y.G.: E-mail: yfgao@shu.edu.cn.

### Notes

The authors declare no competing financial interest.

## ■ ACKNOWLEDGMENTS

This study was supported in part by One-Hundred-Talent Project and the Key Research Program (Grant no. KGZD-EW-T06) of the Chinese Academy of Sciences, NSFC (State Outstanding Young Scholars, 51325203), and the research grant (no. 15XD1501700, 14DZ2261200) from Shanghai Science and Technology Commission.





DOI: 10.1021/acs.jpclett.5b01376
J. Phys. Chem. Lett. 2015, 6, 3650−3656

## REFERENCES


(1) Li, Z.; Hu, Z.; Peng, J.; Wu, C.; Yang, Y.; Feng, F.; Gao, P.; Yang, J.; Xie, Y. Ultrahigh Infrared Photoresponse from Core-Shell Single-Domain-$VO_2$/$V_2O_5$ Heterostructure in Nanobeam. *Adv. Funct. Mater.* **2014**, *24*, 1821−1830.

(2) Wu, C.; Dai, J.; Zhang, X.; Yang, J.; Qi, F.; Gao, C.; Xie, Y. Direct Confined-Space Combustion Forming Monoclinic Vanadium Dioxides. *Angew. Chem.* **2010**, *122*, 138−141.

(3) Wu, C.; Feng, F.; Feng, J.; Dai, J.; Peng, L.; Zhao, J.; Yang, J.; Si, C.; Wu, Z.; Xie, Y. Hydrogen-Incorporation Stabilization of Metallic $VO_2$ (R) Phase to Room Temperature, Displaying Promising Low-Temperature Thermoelectric Effect. *J. Am. Chem. Soc.* **2011**, *133*, 13798−13801.

(4) Zheng, H.; Wagner, L. K. Computation of the Correlated Metal-Insulator Transition in Vanadium Dioxide from First Principles. *Phys. Rev. Lett.* **2015**, *114*, 176401.

(5) Zhou, J.; Gao, Y.; Zhang, Z.; Luo, H.; Cao, C.; Chen, Z.; Dai, L.; Liu, X. $VO_2$ Thermochromic Smart Window for Energy Savings and Generation. *Sci. Rep.* **2013**, *3*, 3029.

(6) Gao, Y.; Wang, S.; Kang, L.; Chen, Z.; Du, J.; Liu, X.; Luo, H.; Kanehira, M. $VO_2$-Sb:$SnO_2$ Composite Thermochromic Smart Glass Foil. *Energy Environ. Sci.* **2012**, *5*, 8234−8237.

(7) Kumar, S.; Strachan, J. P.; Pickett, M. D.; Bratkovsky, A.; Nishi, Y.; Williams, R. S. Sequential Electronic and Structural Transitions in $VO_2$ Observed Using X-ray Absorption Spectromicroscopy. *Adv. Mater.* **2014**, *26*, 7505−7509.

(8) Yao, T.; Zhang, X.; Sun, Z.; Liu, S.; Huang, Y.; Xie, Y.; Wu, C.; Yuan, X.; Zhang, W.; Wu, Z.; et al. Understanding the Nature of the Kinetic Process in A $VO_2$ Metal-Insulator Transition. *Phys. Rev. Lett.* **2010**, *105*, 226405.

(9) Wu, C.; Feng, F.; Xie, Y. Design of Vanadium Oxide Structures with Controllable Electrical Properties for Energy Applications. *Chem. Soc. Rev.* **2013**, *42*, 5157−5183.

(10) Hu, B.; Ding, Y.; Chen, W.; Kulkarni, D.; Shen, Y.; Tsukruk, V. V.; Wang, Z. L. External-Strain Induced Insulating Phase Transition in $VO_2$ Nanobeam and Its Application as Flexible Strain Sensor. *Adv. Mater.* **2010**, *22*, 5134−5139.

(11) Goodenough, J. B. The Two Components of the Crystallographic Transition in $VO_2$. *J. Solid State Chem.* **1971**, *3*, 490−500.

(12) Qazilbash, M. M.; Brehm, M.; Chae, B.-G.; Ho, P.-C.; Andreev, G. O.; Kim, B.-J.; Yun, S. J.; Balatsky, A. V.; Maple, M. B.; Keilmann, F.; et al. Mott Transition in $VO_2$ Revealed by Infrared Spectroscopy and Nano-Imaging. *Science* **2007**, *318*, 1750−1753.

(13) Kim, H.-T.; Lee, Y. W.; Kim, B.-J.; Chae, B.-G.; Yun, S. J.; Kang, K.-Y.; Han, K.-J.; Yee, K.-J.; Lim, Y.-S. Monoclinic and Correlated Metal Phase in $VO_2$ as Evidence of the Mott Transition: Coherent Phonon Analysis. *Phys. Rev. Lett.* **2006**, *97*, 266401.

(14) Booth, J. M.; Casey, P. S. Anisotropic Structure Deformation in the $VO_2$ Metal-Insulator Transition. *Phys. Rev. Lett.* **2009**, *103*, 086402.

(15) Haverkort, M. W.; Hu, Z.; Tanaka, A.; Reichelt, W.; Streltsov, S. V.; Korotin, M. A.; Anisimov, V. I.; Hsieh, H. H.; Lin, H. J.; Chen, C. T.; Khomskii, D. I.; et al. Orbital-Assisted Metal-Insulator Transition in $VO_2$. *Phys. Rev. Lett.* **2005**, *95*, 196404.

(16) Cavalleri, A.; Dekorsy, T.; Chong, H. H. W.; Kieffer, J. C.; Schoenlein, R. W. Evidence for A Structurally-Driven Insulator-to-Metal Transition in $VO_2$: A View from the Ultrafast Timescale. *Phys. Rev. B: Condens. Matter Mater. Phys.* **2004**, *70*, 161102.

(17) Koethe, T. C.; Hu, Z.; Haverkort, M. W.; Schüßler-Langeheine, C.; Venturini, F.; Brookes, N. B.; Tjernberg, O.; Reichelt, W.; Hsieh, H. H.; Lin, H. J.; et al. Transfer of Spectral Weight and Symmetry across the Metal-Insulator Transition in $VO_2$. *Phys. Rev. Lett.* **2006**, *97*, 116402.

(18) Gao, Y.; Wang, S.; Luo, H.; Dai, L.; Cao, C.; Liu, Y.; Chen, Z.; Kanehira, M. Enhanced Chemical Stability of $VO_2$ Nanoparticles by the Formation of $SiO_2$/$VO_2$ Core/Shell Structures and the Application to Transparent and Flexible $VO_2$-Based Composite Foils with Excellent Thermochromic Properties for Solar Heat Control. *Energy Environ. Sci.* **2012**, *5*, 6104−6110.

(19) Bae, S.-H.; Lee, S.; Koo, H.; Lin, L.; Jo, B. H.; Park, C.; Wang, Z. L. The Memristive Properties of A Single $VO_2$ Nanowire with Switching Controlled by Self-Heating. *Adv. Mater.* **2013**, *25*, 5098−5103.

(20) Lee, S.; Cheng, C.; Guo, H.; Hippalgaonkar, K.; Wang, K.; Suh, J.; Liu, K.; Wu, J. Axially Engineered Metal−Insulator Phase Transition by Graded Doping $VO_2$ Nanowires. *J. Am. Chem. Soc.* **2013**, *135*, 4850−4855.

(21) Yuan, X.; Zhang, Y.; Abtew, T. A.; Zhang, P.; Zhang, W. $VO_2$:Orbital Competition, Magnetism, and Phase Stability. *Phys. Rev. B: Condens. Matter Mater. Phys.* **2012**, *86*, 235103.

(22) Eyert, V. $VO_2$: A Novel View from Band Theory. *Phys. Rev. Lett.* **2011**, *107*, 016401.

(23) Iori, F.; Gatti, M.; Rubio, A. Role of Nonlocal Exchange in the Electronic Structure of Correlated Oxides. *Phys. Rev. B: Condens. Matter Mater. Phys.* **2012**, *85*, 115129.

(24) Yuan, X.; Zhang, W.; Zhang, P. Hole-Lattice Coupling and Photoinduced Insulator-Metal Transition in $VO_2$. *Phys. Rev. B: Condens. Matter Mater. Phys.* **2013**, *88*, 035119.

(25) Wei, J.; Ji, H.; Guo, W.; Nevidomskyy, A. H.; Natelson, D. Hydrogen Stabilization of Metallic Vanadium Dioxide in Single-Crystal Nanobeams. *Nat. Nanotechnol.* **2012**, *7*, 357−362.

(26) Liebsch, A.; Ishida, H.; Bihlmayer, G. Coulomb Correlations and Orbital Polarization in the Metal-Insulator Transition of $VO_2$. *Phys. Rev. B: Condens. Matter Mater. Phys.* **2005**, *71*, 085109.

(27) Chen, S.; Liu, J.; Wang, L.; Luo, H.; Gao, Y. Unraveling Mechanism on Reducing Thermal Hysteresis Width of $VO_2$ by Ti Doping: A Joint Experimental and Theoretical Study. *J. Phys. Chem. C* **2014**, *118*, 18938−18944.

(28) Laad, M. S.; Craco, L.; Müller-Hartmann, E. Metal-insulator Transition in Rutile-Based $VO_2$. *Phys. Rev. B: Condens. Matter Mater. Phys.* **2006**, *73*, 195120.

(29) Biermann, S.; Poteryaev, A.; Lichtenstein, A. I.; Georges, A. Dynamical Singlets and Correlation-Assisted Peierls Transition in $VO_2$. *Phys. Rev. Lett.* **2005**, *94*, 026404.

(30) Gatti, M.; Bruneval, F.; Olevano, V.; Reining, L. Understanding Correlations in Vanadium Dioxide from First Principles. *Phys. Rev. Lett.* **2007**, *99*, 266402.

(31) Sakuma, R.; Miyake, T.; Aryasetiawan, F. First-Principles Study of Correlation Effects in $VO_2$. *Phys. Rev. B: Condens. Matter Mater. Phys.* **2008**, *78*, 075106.

(32) Pintchovski, F.; Glaunsinger, W. S.; Navrotsky, A. Experimental Study of the Electronic and Lattice Contributions to the $VO_2$ Transition. *J. Phys. Chem. Solids* **1978**, *39*, 941−949.

(33) Takanashi, K.; Yasuoka, H.; Ueda, Y.; Kosuge, K. NMR Studies of $VO_2$ and $V_{1-x}W_xO_2$. *J. Phys. Soc. Jpn.* **1983**, *52*, 3953−3959.

(34) Kresse, G.; Furthmüller, J. Efficient Iterative Schemes for Ab Initio Total-Energy Calculations using A Plane-Wave Basis Set. *Phys. Rev. B: Condens. Matter Mater. Phys.* **1996**, *54*, 11169−11186.

(35) Kresse, G.; Furthmüller, J. Efficiency of Ab-Initio Total Energy Calculations for Metals and Semiconductors using A Plane-Wave Basis Set. *Comput. Mater. Sci.* **1996**, *6*, 15−50.

(36) Pickett, W. E.; Erwin, S. C.; Ethridge, E. C. Reformulation of the LDA+U Method for A Local-Orbital Basis. *Phys. Rev. B: Condens. Matter Mater. Phys.* **1998**, *58*, 1201−1209.

(37) Rogers, K. D. An X-ray Diffraction Study of Semiconductor and Metallic Vanadium Dioxide. *Powder Diffr.* **1993**, *8*, 240−244.

(38) Ladd, L. A.; Paul, W. Optical and Transport Properties of High Quality Crystals of $V_2O_4$ Near the Metallic Transition Temperature. *Solid State Commun.* **1969**, *7*, 425−428.

(39) Sohn, J. I.; Joo, H. J.; Kim, K. S.; Yang, H. W.; Jang, A.-R.; Ahn, D.; Lee, H. H.; Cha, S.; Kang, D. J.; Kim, J. M.; et al. Stress-Induced Domain Dynamics and Phase Transitions in Epitaxially Grown $VO_2$ Nanowires. *Nanotechnology* **2012**, *23*, 205707.

(40) Tan, X.; Yao, T.; Long, R.; Sun, Z.; Feng, Y.; Cheng, H.; Yuan, X.; Zhang, W.; Liu, Q.; Wu, C.; et al. Unraveling Metal-Insulator Transition Mechanism of $VO_2$ Triggered by Tungsten Doping. *Sci. Rep.* **2012**, *2*, 466.






DOI: 10.1021/acs.jpclett.5b01376
*J. Phys. Chem. Lett.* 2015, 6, 3650−3656

(41) Liu, M.; Hwang, H. Y.; Tao, H.; Strikwerda, A. C.; Fan, K.; Keiser, G. R.; Sternbach, A. J.; West, K. G.; Kittiwatanakul, S.; Lu, J.; et al. Terahertz-Field-Induced Insulator-to-Metal Transition in Vanadium Dioxide Metamaterial. *Nature* **2012**, *487*, 345−348.
(42) Béteille, F.; Livage, J. Optical Switching in $VO_2$ Thin Films. *J. Sol-Gel Sci. Technol.* **1998**, *13*, 915−921.
(43) Chang, S.-J.; Park, J. B.; Lee, G.; Kim, H. J.; Lee, J.-B.; Bae, T.-S.; Han, Y.-K.; Park, T. J.; Huh, Y. S.; Hong, W.-K. In Situ Probing of Doping- and Stress-mediated Phase Transitions in A Single-Crystalline $VO_2$ Nanobeam by Spatially Resolved Raman Spectroscopy. *Nanoscale* **2014**, *6*, 8068−8074.
(44) Ji, Y.; Zhang, Y.; Gao, M.; Yuan, Z.; Xia, Y.; Jin, C.; Tao, B.; Chen, C.; Jia, Q.; Lin, Y. Role of Microstructures on the M1-M2 Phase Transition in Epitaxial $VO_2$ Thin Films. *Sci. Rep.* **2014**, *4*, 4854.





DOI: 10.1021/acs.jpclett.5b01376
*J. Phys. Chem. Lett.* 2015, 6, 3650−3656